Casting of Diffusion-Controlled Free Radical Polymerization—Experimental and Theoretical Analysis

Y. J. HUANG, J. D. FAN, and L. J. LEE,* *Department of Chemical Engineering, The Ohio State University, Columbus, Ohio 43210*

Synopsis

This paper is concerned with applications of a kinetic-diffusion model which accounts for the gel effect and glass effect for free radical polymerizations under nonisothermal conditions. Bulk polymerizations of styrene and unsaturated polyester in the batch casting process were investigated both experimentally and theoretically. A differential scanning calorimeter (DSC) and a Fourier transform infrared spectrometer (FTIR) were employed to elucidate incomplete reactions resulting from glass transition and dead-ending phenomena and to provide kinetic information for modelling. Temperature, conversion, and cumulative molecular weight profiles were simulated under several wall temperature programs. Predictions of ultimate cumulative molecular weights across the reactor, when compared with experimental results measured by gel permeation chromatography (GPC), affirmed that the molecular weight variation due to the radial temperature gradient could be alleviated by manipulating the wall temperature.

INTRODUCTION

A large number of polymer products are formed into their final shape by polymerization. Examples are reaction injection molding (RIM), compression molding of sheet molding compounds (SMC), and monomer casting, to mention a few. Problems of nonuniform reaction in the mold or reactor due to heat transfer and reaction exotherm have been recognized by many researchers.[1-5] For the free radical bulk polymerization, it is well known that the exothermic nature of the reaction together with the inferior heat transfer characteristics of polymers frequently leads to thermal runaway phenomenon,[6-10] the manifestations of which, for instance, are "hot spots" and "peaking" in batch reactors and "hot streamlines" in continuous reactors. Quite often, undesirable product properties, such as low ultimate monomer conversion owing to depletion of initiator (dead-ending),[11] low degree of polymerization, and broad molecular weight distribution, result concomitantly. The hot spots associated with the thermal runaway are attributed to two distinct mechanisms, namely, the rapid formation of the radical population at the beginning of the reaction and the Trommsdorff or gel effect.[12-15]

Biesenberger et al.[7-9] have proposed the theory of "thermal ignition" for the chain addition polymerization and worked out computational and experimental cases for the batch styrene polymerization with various initiators.

* To whom correspondence should be addressed.

Journal of Applied Polymer Science, Vol. 33, 1315–1341 (1987)
 CCC 0021-8995/87/041315-27$04.00

They define thermal ignition as the condition where the reaction temperature increases rapidly with time and the rate of increase in temperature also increases with time (i.e., a concave upward curve). Their theory, computations, and experiments were for well-stirred batch reactors known as lumped parameter systems with constant heat transfer coefficients. The theory has later been extended to distributed parameter systems[10] in which the temperature is a spatial variable. Their work is of interest for understanding the boundaries of stability for abnormal situations like initiator mischarge or control malfunctions.

To achieve good product properties, gel effect, thermal runaway, or thermal ignition experienced by the reaction fluid must be avoided or minimized. Optimal temperature or initiator addition policies that minimize reaction times[16,18-21] or the breadth of the molecular weight distribution[17,22] for chain addition polymerizations in homogeneous batch reactors have been presented. For distributed parameter systems, extensive studies[23-33] have carried out to test the operability of tubular reactors and to elucidate the variations of temperature, monomer conversion, velocity, and product properties across the tube as a result of changes in feed conditions, wall temperature, coolant temperature, or tube diameter.

The purpose of this study is to investigate the batch casting process for styrene and unsaturated polyester resin using a recently developed kinetic-diffusion model.[15] The work describes the experiments and theoretical simulation used to obtain kinetic information, temperature profile, and molecular weights.

EXPERIMENTAL

Materials

The unsaturated polyester paste and styrene used are listed in Table I. The former contains styrene and an unsaturated polyester resin which is a 1 : 1 propylene–maleate polyester combined with 35% by weight of styrene (P-325, Owens Corning Fiberglas). This resin is a typical ingredient used in the automotive grade sheet molding compound. Calcium carbonate ($CaCO_3$) was

TABLE I
Polyester Paste and Styrene Used in This Study

Ingredient	Parts by weight	
	Polyester paste	Styrene
Styrene	33.0	100
65% Unsaturated polyester in styrene (P-325)	67.0	—
Filler $CaCO_3$[a]	103.0	—
Initiator AIBN	3.0	—
Initiator BPO	—	3.0
Inhibitor BQ	—	0.26

[a] Only added during casting.

added therein to act both as heat conductor and heat sink during the casting experiment.[4] The former role improved the heat transfer between the mold wall and the reacting system while the latter reduced the temperature rise and gradient inside the mold. 2,2′-Azobisisobutyronitrile (AIBN) was used as an initiator for the highly crosslinking polyester system. All materials were used as received.

As to the other system, styrene was first freed of inhibitor by the usual procedures.[34] Three parts of initiator, benzoyl peroxide (BPO), and 0.26 part of benzoquinone (BQ), were than added to the monomer. All materials were prepared and stored in a refrigerator for no more than 24 h before the experiments to avoid any premature reaction.

Instrumentation and Experimental Procedures

Kinetic Measurement

For the kinetic study, a differential scanning calorimeter (DSC-2C, Perkin-Elmer) was used to measure the rate of heat released during the polymerization. The DSC was first set isothermally at prespecified temperature, then one or two drops of mixture, weighing from 10 to 25 mg, were put into a preweighed sample pan. The pan was tightly sealed and loaded into the DSC. The sample pan used was either a volatile pan made of aluminum, which was capable of withstanding at least 30 psia (207 kPa) internal pressure after sealing, or a large volume capsule made of stainless steel, which was designed to have O-ring inside with the capability of suppressing the vaporization of monomer during the experiment. Isothermal DSC runs were ended when there was no further exotherm. Samples were then reheated from room temperature to 200°C in the scanning mode with a heating rate of 5°C/min to determine the residual exotherm left in the isothermally cured samples. The total heat of reaction was calculated from areas under both isothermal and scanning DSC curves. The exothermic curve during the reaction was then allowed to yield the reaction rate profile as well as the final (limiting) conversion.[35] Isothermal reaction rate vs. time profiles were measured at four temperatures, 60, 70, 80, and 90°C, for the polyester resin and three temperatures, 80 90, and 100°C, for the styrene reaction.

DSC has the advantages of simplicity, less limitation, and the capacity to yield simultaneously information regarding kinetics, energetics, and thermal properties. However, it tends to be less accurate due to its lack of detail in the kinetic sense and less sensitive at high conversions, especially if there exists a permanent residue since the measurement relys on the reaction exotherm. Therefore, a Fourier transform infrared spectrometer (FTIR) (Model 20-DX, Nicolet) with a resolution of 4 cm^{-1} was employed to study the reaction kinetics of polyester resin at high conversions since the polyester resin showed a strong residual reactivity in the DSC measurement. One drop of the mixture was dispersed between two sodium chloride plates. The plates were tightly sealed in a brass tube which was then immersed in a temperature-controlled oil bath for 8 h. After reaction, the plates were mounted on the sample holder located in the FTIR, and 10 consecutive scans were taken to produce the IR

spectrum for the reacted sample. Peak height method was used to calculate the amount of unreacted monomers left in the system, which was in contrast to the principle used in the DSC measurement since DSC detected the amount of monomer reacted. Three temperatures, 60, 105, and 121°C, were used in the FTIR experiments.

Batch Casting

For the casting experiments, a glass tube of 6 in. long and 3/4 in. in diameter (Fig. 1) was filled with material and sealed with a rubber plug. The tube, which was immersed in a temperature-controlled oil bath, was tightly clamped to suppress the vaporization of monomer during the casting process. Two thermocouples (Type J, Omega) were inserted along the tube through the rubber plug and located at midportion of the tube to record temperature profiles at the center line and near the wall. At the end of experiment, the tube was cut off around the midsection, and some material was scraped and collected for further analysis. The molecular weights and molecular weight distribution were obtained by gel permeation chromatography (GPC, Perkin-Elmer, with five microstyrogel columns, 10^2, 10^3, 10^4, 10^5 and 10^6), while the final (limiting) conversion was measured by using DSC. Five wall temperature programs, namely 75, 90, 75–90, 90–75–90, and 75–60–90°C, were conducted in the batch casting experiments where the first temperature switchover was around the onset of gel effect at the center and the second one was after the maximum temperature rise. The details will be given in the later sections.

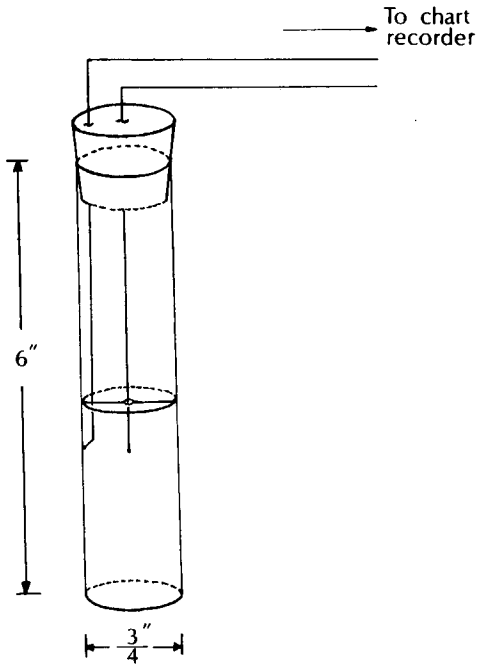

Fig. 1. Schematic of the experimental set-up used for the casting study.

RESULTS AND DISCUSSION

Kinetics

DSC curves of reaction rate vs. time for styrene reactions[15] in the isothermal mode are shown in Figure 2. In general, the reaction started after an induction time and reached the first maximum rate immediately. The rate decreased in the early period of reaction primarily due to the consumption of monomers, and then climbed up to the second maximum point due to the well-known gel effect. Finally, the reaction rate decayed rapidly to zero because of the transition of the polymer–monomer system from a viscous liquid to a glassy solid. After the isothermal reaction, no exothermic peak was observed during the scanning run, which suggests that styrene polymerization was complete under the given isothermal condition (i.e., 80–100°C).

Unlike the styrene reaction, the rate profile of polyester reaction shows only one peak (see Fig. 3) This arises from the fact that[15] each unsaturated polyester molecule, on the average, has 10 or more double bonds,[36] which caused an early onset of gelation and most of the reaction proceeded in the solid state. As a consequence, the reaction was affected by the diffusion effect through almost the entire reaction course, and thereby only one peak was observed. Scanning of the cured samples indicated that the conversion was incomplete for isothermal runs in the temperatures ranging from 60 to 90°C. Figure 4 shows the incomplete reaction for those isothermal runs. The amount of residual reactivity together with the induction time t_z and heat of reaction for all the isothermal experiments is listed in Table II.

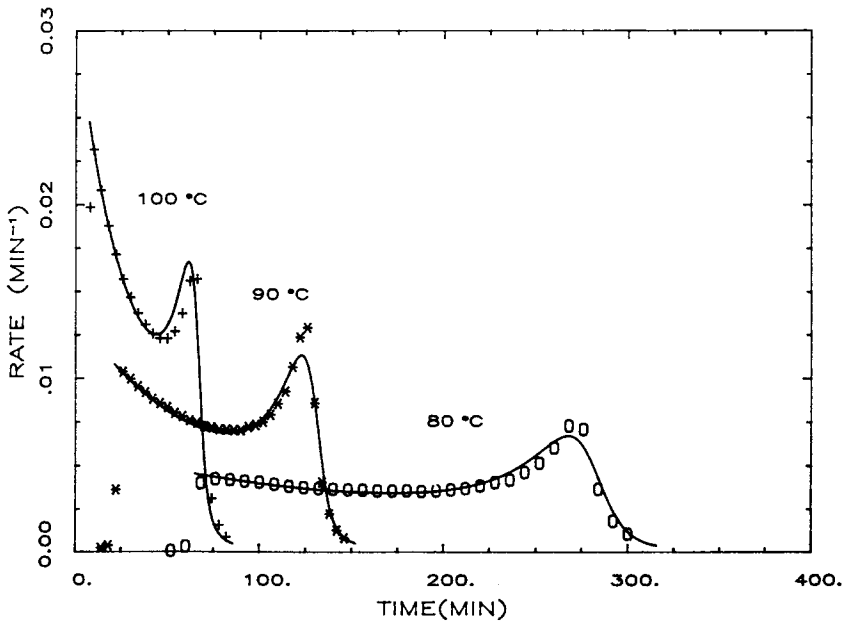

Fig. 2. Isothermal DSC curves for styrene reaction. (—) model prediction; (symbols) experimental data.

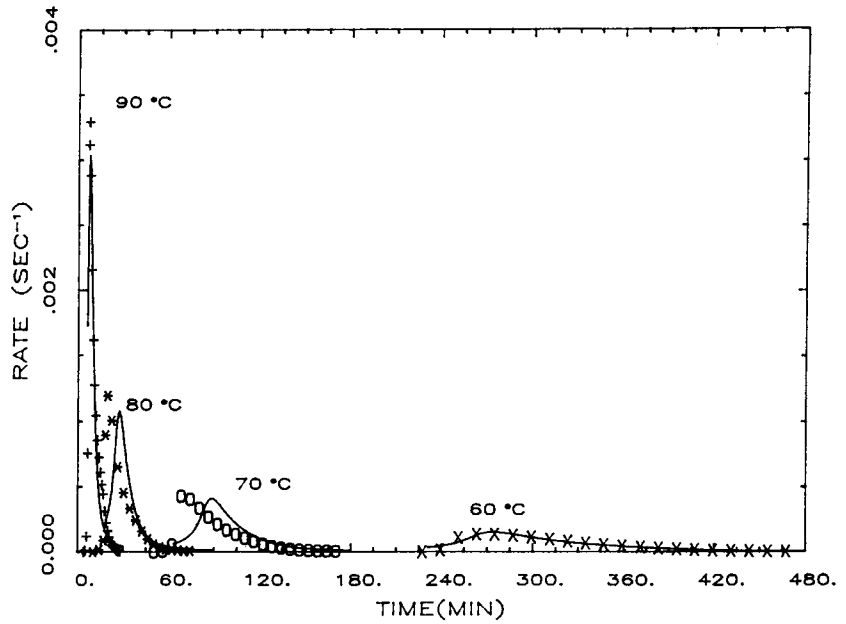

Fig. 3. Isothermal DSC curves for polyester reaction. (—) model prediction; (symbols) experimental data.

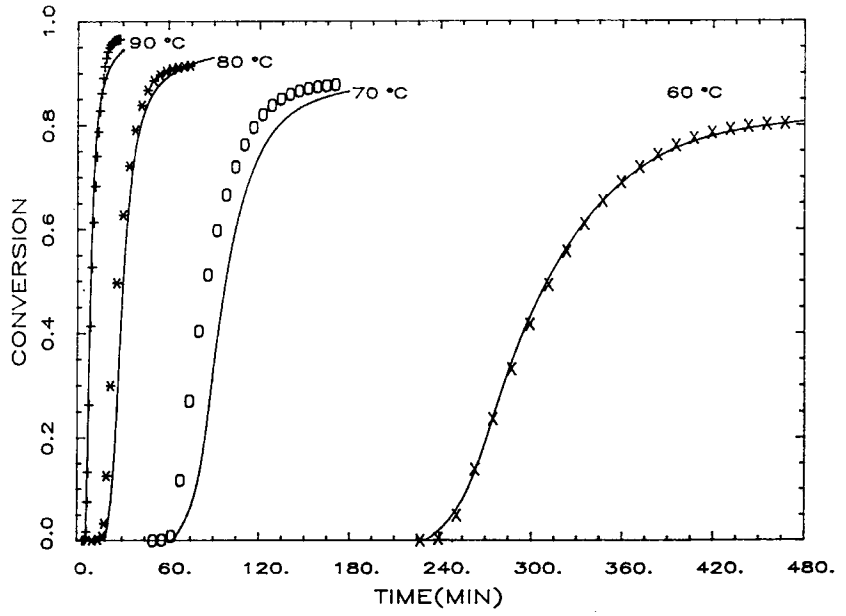

Fig. 4. Conversion vs. time for isothermal polyester reaction. (—) model prediction; (symbols) experimental data.

TABLE II
Summary of Isothermal DSC Runs for Polyester and Styrene Reactions

Temp (°C)	t_z (min)	Limiting conversion α (%)	ΔH_R (cal/g)
		a. Polyester reaction	
60	227.2	80.4	80.6
70	50.2	88.0	87.0
80	10.2	91.6	87.5
90	3.9	96.6	79.0
		b. Styrene reaction[15]	
80	64.8	~ 100	158.5
90	21.6	100	151.2
100	7.4	100	158.0

A typical FTIR result for polyester reaction is given in Figure 5 where four IR spectra, one before the reaction and the other three after 8 h of reaction at 60, 105, and 121°C, respectively, are plotted together. The decrease of the styrene C=C bonds due to the styrene homopolymerization and the copolymerization of styrene and polyester was followed by a peak at the wave number of 912. It can be seen from Figure 5 that at 60°C there was a substantial amount of unreacted C=C bonds, which indicated that reaction was less than completion at this temperature. Increasing the reaction temperature to 105°C reduced the residual peak. However, further increase of the reaction temperature to 121°C exhibited a larger residual height, which revealed a decrease of the final (limiting) conversion. Figure 6 shows the temperature effect on the limiting conversion measured by both DSC and FTIR. For temperatures higher than 90°C, the reaction is too fast to be followed by DSC. Only FTIR was used at high temperatures. It can be explained that at low temperatures the incomplete reaction is due to the glass effect while at high temperatures to the dead-ending phenomenon. At low temperatures, increasing temperature may reduce the glass effect and, in turn, enhance the conversion. However, at too high a temperature where the dead-ending predominates, the conversion may decline. For the polyester system with AIBN as an initiator, the reaction was always less than completion. If the final conversion is a major concern of the process, a high temperature initiator or multiple initiators should be employed. Figure 6 shows that the limiting conversion measured by FTIR is lower than that by DSC. This demonstrates that DSC measurement is relatively insensitive at high conversions since it measures the reaction exotherm instead of the functional group itself.

Batch Casting

Figure 7 shows typical temperature vs. time profiles for the casting of polyester resin with the wall temperature at 70°C (the dotted line is experimental data). Initially, the temperature increase was mainly due to the heat input from the wall. Following this was a sharp temperature rise caused by reaction exotherm during the fast free radical polymerization. Finally, concluding the profile was a period during which heat transferred out from the

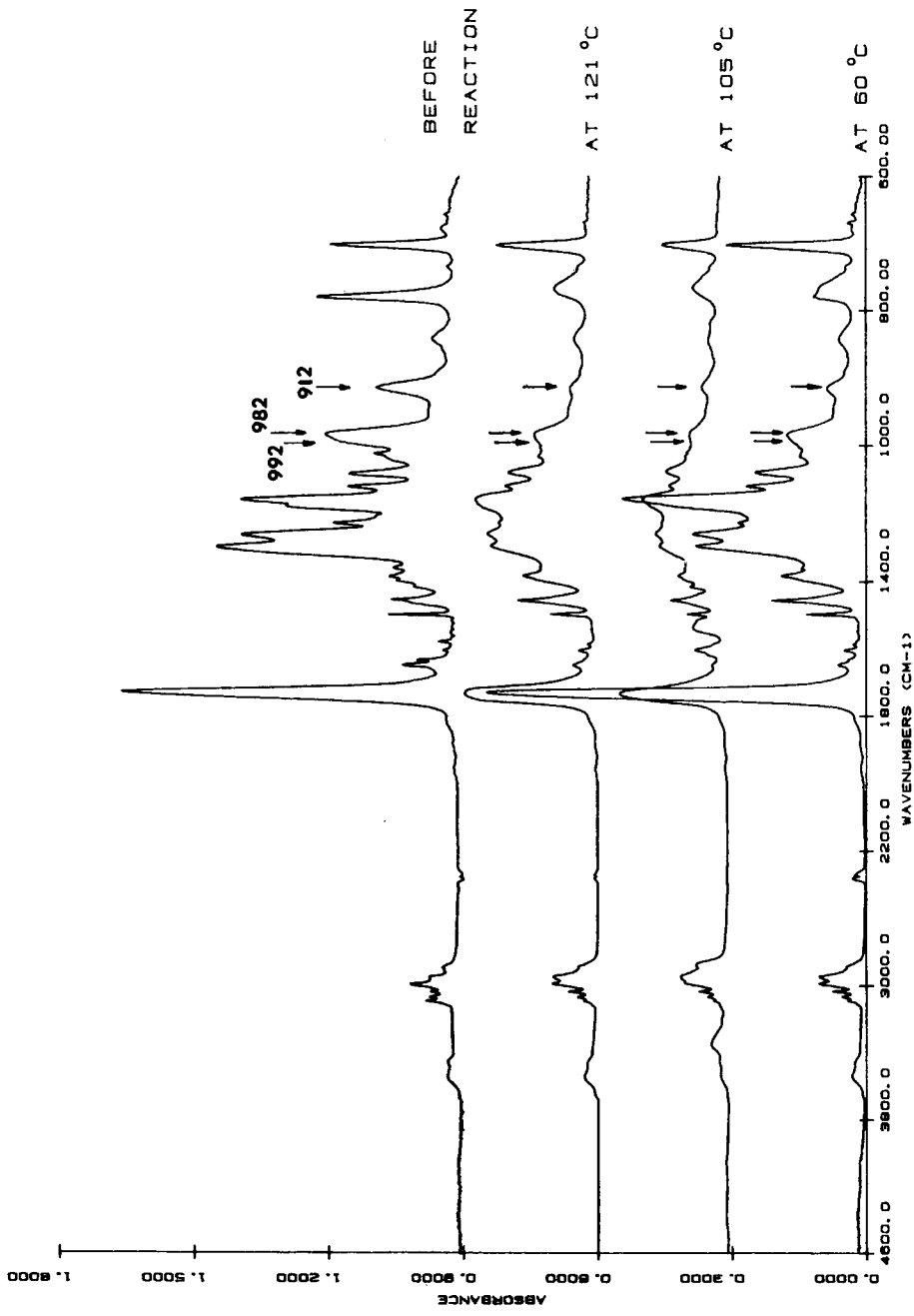

Fig. 5. Absorbance vs. wavenumber of FTIR spectra for polyester reaction, before and after 8 h at 60, 105, and 121°C.

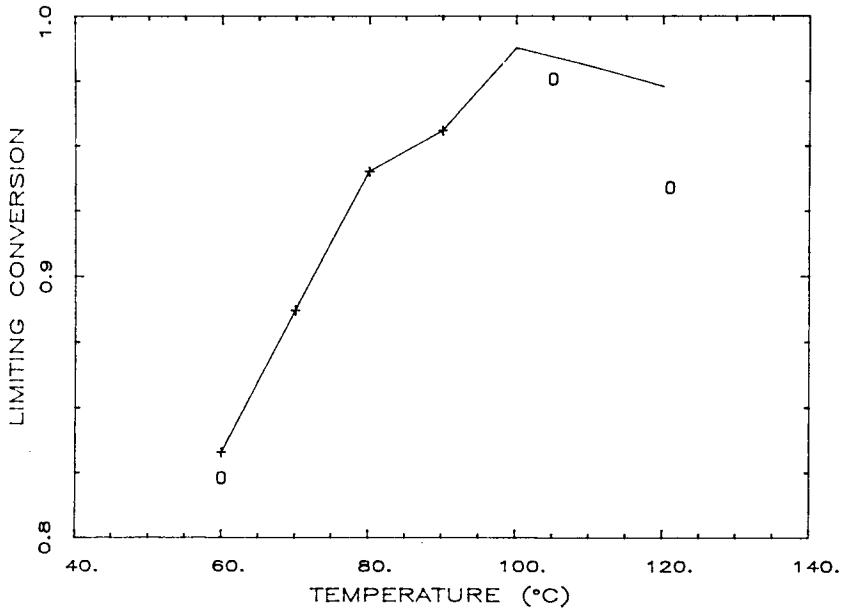

Fig. 6. Effect of temperature on limiting conversion for polyester reaction initiated by AIBN: (—) model prediction; (+) experimental data by DSC; (○) experimental data by FTIR.

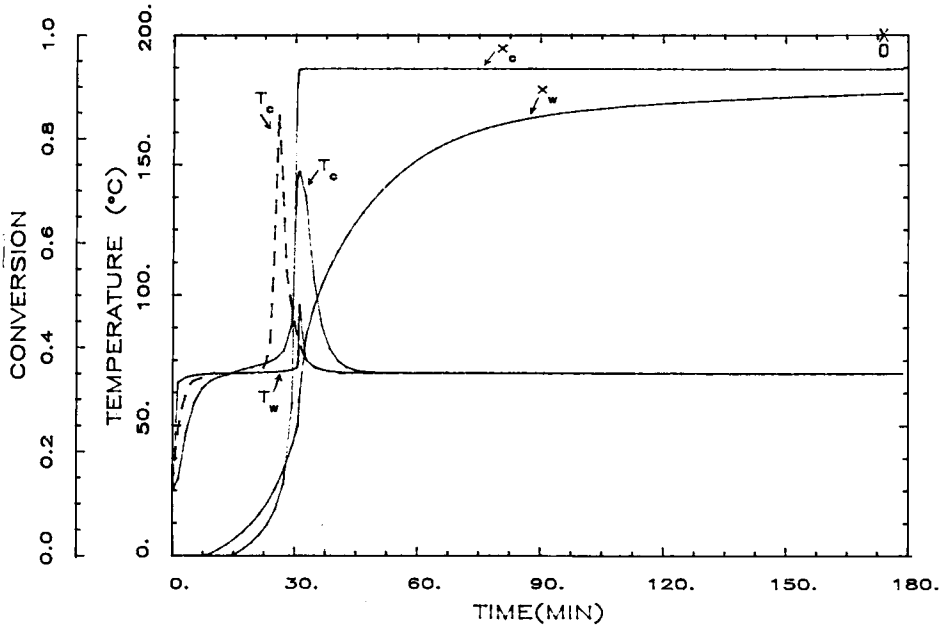

Fig. 7. Local temperature and conversion profiles for the casting of polyester resin. T_w = 70°C diameter = 3/4 in.: (—) model prediction; (---) experimental data; (×) experimental limiting conversion at the center; (○) experimental limiting conversion near the wall.

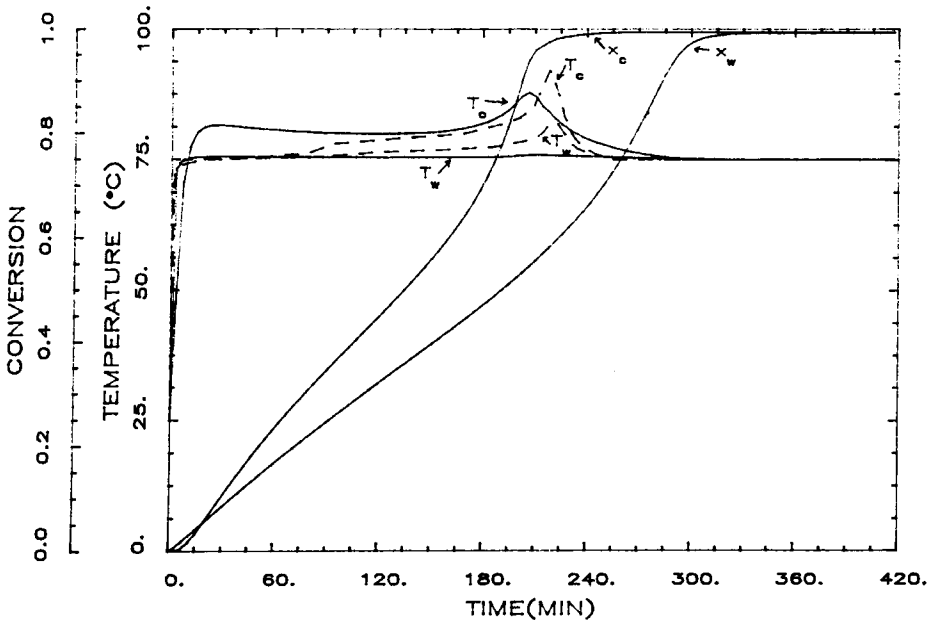

Fig. 8. Local temperature and conversion profiles for the casting of styrene. $T_w = 75°C$ diameter = 3/4 in.: (—) model prediction; (---) experimental data.

reacted polymer through the wall. For the material cured near the wall, the temperature changes were moderated by heat exchange with the mold wall. The final conversion measured by DSC indicated that the reaction near the wall was incomplete, which was presumably due to the glass effect. Figure 8 shows typical temperature profiles for the casting of styrene at 75°C, which resembles the rate profiles measured under isothermal conditions (Fig. 2). The temperature profile experienced two peaks. The first peak resulted from the initial reaction exotherm of styrene polymerization, while the second peak indicated the onset of gel effect. DSC results showed that the reaction was completed both at the center and near the wall.

Figure 9 shows the temperature curves for other wall temperature programs. In the case of 75–90°C, the wall temperature was raised to 90°C as soon as the center temperature reached its maximum, while, in the cases of 75–60–90°C and 90–75–90°C, the first temperature switchover occurred near the onset of the gel effect at the center and second one occurred after the second temperature peak. The purpose of the wall temperature changes was to reduce the reaction time without sharply increasing the maximum temperature reached in the mold. Table III, however, shows that the maximum temperature at the center could rise to as high as 150°C. Table III also summarizes measured molecular weights and molecular weight distributions for the casted polystyrene samples under different wall temperature programs. Owing to the high initiator concentration employed, which was about 0.1*M*, the molecular weights obtained were less than those of the typical commercial polystyrene resins. Generally speaking, at constant wall temperatures, either 75 or 90°C, the molecular weights were higher near the wall than at the center as expected. For the case of 75–90°C wall temperature, the variation of

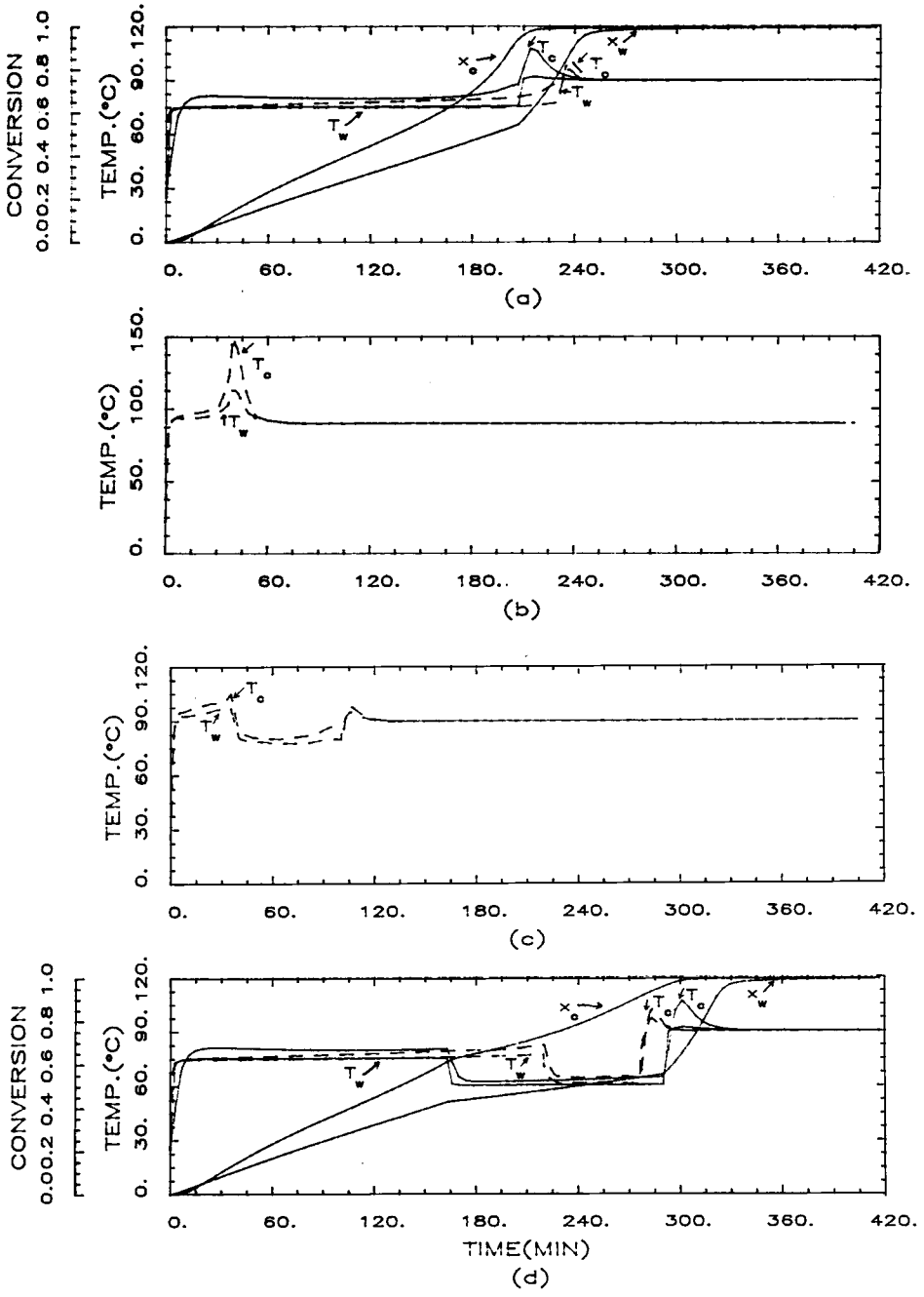

Fig. 9. Local temperature and conversion profiles for the casting of styrene. Diameter = 3/4 in.: (a) T_w = 75–90°C; (b) T_w = 90°C; (c) T_w = 90–75–90°C; (d) T_w = 75–60–90°C; (—) model prediction; (---) experimental data.

TABLE III
Measured Maximum Temperature and Molecular Weights of Casted Polystyrene under Different Wall Temperature Programs

Wall temp (°C)		Experiment				Simulation		
		$\langle \bar{M}_w \rangle \times 10^4$	$\langle \bar{M}_n \rangle \times 10^4$	$\langle \bar{M}_w \rangle / \langle \bar{M}_n \rangle$	T_{max}	$\langle \bar{M}_w \rangle \times 10^4$	$\langle \bar{M}_n \rangle \times 10^4$	$\langle \bar{M}_w \rangle / \langle \bar{M}_w \rangle$
75	Center	4.7	1.8	2.6	92	4.0	2.2	1.8
	Wall	4.8	2.0	2.4	—	5.9	3.1	1.9
75–90	Center	4.8	2.3	2.1	102	4.0	1.3	3.0
	Wall	4.0	1.7	2.4	—	3.6	1.3	2.7
90	Center	2.7	1.4	1.9	150	1.6[a]	1.0[a]	1.6[a]
	Wall	3.5	1.5	2.3		3.9[a]	2.1[a]	1.9[a]
90–75–90	Center	2.9	1.4	2.1	105	—	—	—
	Wall	3.9	1.6	2.4	—	—	—	—
75–60–90	Center	4.8	2.0	2.4	102	9.4	1.5	6.3
	Wall	5.2	2.1	2.5	—	4.3	1.4	3.0

[a]Wall temperature was maintained at 85°C.

molecular weights in the radial direction was reversed with a higher molecular weight at the center than near the wall. For other wall temperature programs including 90–75–90 and 75–60–90°C, the molecular weights at the center were dominated by the wall temperature in the first period and were insensitive to the later temperature changes. On the other hand, the molecular weight near the wall showed a strong dependence on the wall temperatures in the second and third periods.

THEORETICAL ANALYSIS

Kinetics

Recently, we have presented a kinetic-diffusion model for free radical polymerizations.[15] In that work, the usually accepted reaction mechanism was employed.

Initiation:

$$I \xrightarrow{k_d} 2R\cdot$$

$$R\cdot + M \xrightarrow{k_i} M_i\cdot \qquad k_i \gg k_d$$

Inhibition:

$$M_n\cdot + Z \xrightarrow{k_z} P_n + Z\cdot \tag{1}$$

Propagation:

$$M_n\cdot + M \xrightarrow{k_p} M_{n+1}\cdot$$

Termination:

$$M_n \cdot + M_m \cdot \xrightarrow{k_t} P_{n+m}$$

(combination)

The governing equations can then be written as

Inhibition:

$$qz_0 = 2fI_0\left[1 - \exp\left(-\int_0^{t_z} k_d\, dt\right)\right] = 2f(I_0 - \bar{I}_0) \tag{2}$$

Propagation:

$$dM/dt = -k_p M\, M \cdot \quad \text{or} \quad d\alpha/dt = k_p(1-\alpha)M \cdot \tag{3}$$

Termination:

$$dM \cdot /dt = 2fk_d I - k_t M^2 \cdot \tag{4}$$

The apparent propagation rate resistance, $1/k_p$, and the apparent termination rate resistance, $1/k_t$, can be expressed as a combination of kinetic resistance and diffusion resistance[14,15]

$$1/k_p = 1/k_{p0} + A'M \cdot /D_M \tag{5}$$

$$1/k_t = 1/k_{t0} + A''M \cdot /D_P \tag{6}$$

By invoking Bueche's free volume theory, the diffusion coefficient can be expressed as a function of the free volume fraction V_f:

$$D_M = A'_M \exp(-B_M/V_f) \tag{7}$$

$$D_P = A'_P \exp(-B_P/V_f) \tag{8}$$

To obtain a single rate expression, the quasisteady state assumption[37] for free radicals, namely $dM \cdot /dt = 0$, is used, and

$$M \cdot = (2fk_d I/k_t)^{1/2} \tag{9}$$

The final rate expression takes on the form

$$\frac{d\alpha}{dt} = \frac{1-\alpha}{1\Big/\left\{\left[\pi_1 + (\pi_2\pi_3)^2\right]^{1/2} + \pi_2\pi_3\right\} + \pi_4} \tag{10}$$

where

$$\pi_1 = \frac{2f\bar{I}_0 k_d k_{p0}^2}{(1-\epsilon\alpha)k_{t0}} \exp\left(-\int_{t_z}^{t} k_d\, dt\right) \tag{10a}$$

(kinetic effect on propagation and termination)

$$\pi_2 = A_p/F \exp(B_p/V_f) \tag{10b}$$

(diffusion effect on termination)

$$\pi_3 = \frac{f\bar{I}_0 k_{p0} F k_d}{(1-\epsilon\alpha)} \exp\left(-\int_{t_z}^{t} k_d\, dt\right) \tag{10c}$$

(kinetic effect on propagation)

$$\pi_4 = A_M \exp(B_M/V_f) \tag{10d}$$

(diffusion effect on propagation)

If the true propagation rate constant k_{p0} is known, further kinetic expression on $M\cdot$, k_p, and k_t can be derived via eqs. (5), (7), (9), and (10):

$$M\cdot = \frac{\left[\pi_1 + (\pi_2\pi_3)^2\right]^{1/2} + \pi_2\pi_3}{k_{p0}} \tag{11}$$

$$k_p = \frac{1}{1/k_{p0} + \pi_4 M\cdot} \tag{12}$$

$$k_t = \frac{2fk_d I}{M\cdot^2} \tag{13}$$

where $I = \bar{I}_0 \exp(-\int_{t_z}^{t} k_d\, dt)/(1-\epsilon\alpha)$ is obtained from direct integration of species balance for initiator.

Molecular Weights

Methods used for the calculation of molecular weights and molecular weight distribution have been reviewed extensively by Ray.[38] Most kinetic models[14,39-43] for diffusion-controlled vinyl polymerizations have applied the method of moment for the molecular weight calculation, while other models[44-46] invoked instantaneous kinetic chain length for the calculation. In general, these works fitted conversion and number-average molecular weight data very well, but the prediction of weight average molecular weight was less than satisfactory. Soh and Sundberg[46] claimed that the molecular weight distribution in the diffusion affected reactions does not conform to the Schulz–Flory most probable distribution. To predict the weight-average or higher average molecular weights, chain length dependence of the termination

must be accounted for in the kinetic model.[39,46] However, prediction of molecular weights at high conversions is still far from satisfactory. More effort is needed in this area.

Two well-known methods were used here to calculate the molecular weights during the casting process. Based on Hamielec's work,[44,45] the average molecular weights for termination by combination and chain transfer solely due to monomer are

$$\frac{1}{\bar{X}_n} = \tau + \frac{\beta}{2} \tag{14}$$

$$\bar{X}_w = \frac{2[\tau + 3(\beta/2)]}{(\tau + \beta)^2} \tag{15}$$

and

$$\tau = C_M$$

$$\beta = \frac{2fk_d[I]}{k_p[M\cdot][M]} = \frac{2fk_d[I]}{(d\alpha/dt)\{1/(1-\alpha)\}[M]}$$

$$= \frac{2fk_d[\bar{I}_0]\exp\left(-\int_{t_z}^{t} k_d\,dt\right)}{(d\alpha/dt)[M_0]}$$

where $\bar{X}_n$ is instantaneous number average degree of polymerization, $\bar{X}_w$ is instantaneous weight average degree of polymerization, and C_M is chain transfer constant to monomer. The cumulative molecular weights are given by

$$\langle \bar{M}_n \rangle = \frac{M_0\alpha}{\int_0^\alpha \frac{1}{\bar{X}_n}\,d\alpha} \tag{16}$$

$$\langle \bar{M}_w \rangle = \frac{M_0}{\alpha}\int_0^\alpha \bar{X}_w\,d\alpha \tag{17}$$

where M_0 is the molecular weight of the monomer. Differentiating eqs. (16) and (17), respectively, and rearranging yield

$$\frac{d(\alpha\langle \bar{M}_n \rangle)}{dt} = \frac{d\alpha}{dt}\langle \bar{M}_n \rangle\left(2 - \frac{\langle \bar{M}_n \rangle}{\bar{M}_n}\right) \tag{18}$$

$$\frac{d(\alpha\langle \bar{M}_w \rangle)}{dt} = \frac{d\alpha}{dt}\bar{M}_w \tag{19}$$

where $\bar{M}_n$ is the instantaneous number-average molecular weight and $\bar{M}_w$ is the instantaneous weight-average molecular weight. Either eqs. (16) and (17)

or (18) and (19) can be used to calculate cumulative molecular weights. The relevant initial condition is that at $\alpha = 0$ or $t = 0$, $\langle \overline{M}_n \rangle = \overline{M}_n$ and $\langle \overline{M}_w \rangle = \overline{M}_w$.

Another alternative to calculating cumulative molecular weights is based on the method of moment. Given kinetic scheme in eq. (1) and incorporating the chain transfer to monomer, the species balance equations for the radical and dead polymer are listed in Table IV(a). Assuming the long chain hypothesis and the quasisteady state approximation for the primary radicals, the kinetic equations for the moments of the polymer distribution are given in Table IV(b). The moment equations can be further simplified as listed in Table IV(c) by making the quasisteady state approximation for all radicals and neglecting the volume contraction factor for radicals. The cumulative number average molecular weight and weight average molecular weight are given in Table IV(d). Unlike the first method, the method of moment necessitates the information of k_{p0} in order to calculate k_p and k_t via eqs. (12) and (13), which in turn allow the simultaneous integration of the moment equations.

Heat Transfer

The major assumptions regarding heat transfer during the casting process are as follows:

1. Homogeneous and well mixed reaction system.
2. Heat conduction only in the radial direction.

TABLE IV
Molecular Weight Calculation Based on the Method of Moment

a. Species balance

$$\frac{dR \cdot}{dt} = 2fk_dI - k_iR \cdot M$$

$$\frac{dM_1 \cdot}{dt} = k_iR \cdot M - k_pM_1 \cdot M + k_{tr}M[M \cdot - M_1 \cdot] - k_tM_1 \cdot M \cdot$$

$$\frac{dM_n \cdot}{dt} = k_pM(M_{n-1} \cdot - M_n \cdot) - k_{tr}MM_n \cdot - k_tM_n \cdot M \cdot, \qquad n \geq 2$$

$$\frac{dP_n}{dt} = k_{tr}MM_n \cdot + \frac{1}{2}k_t \sum_{m=1}^{n-1} M_m \cdot M_{n-m} \cdot, \qquad n \geq 2$$

where

$$M \cdot = \sum_{n=1}^{\infty} M_n \cdot$$

b. Moment balance

$$\frac{d\lambda_0}{dt} = 2fk_dI - k_t\lambda_0^2 + \frac{\lambda_0^2\epsilon(1-\alpha)}{1-\epsilon\alpha}k_p$$

$$\frac{d\lambda_1}{dt} = 2fk_dI - k_t\lambda_0\lambda_1 + k_p\lambda_0[M_0]\frac{1-\alpha}{1-\epsilon\alpha} + \frac{k_{tr}[M_0](1-\alpha)}{(1-\epsilon\alpha)}(\lambda_0 - \lambda_1) + \frac{\lambda_0\lambda_1\epsilon(1-\alpha)}{1-\epsilon\alpha}k_p$$

TABLE IV *(Continued from the previous page.)*

$$\frac{d\lambda_2}{dt} = 2fk_dI - k_t\lambda_0\lambda_2 + k_p[M_0]\frac{1-\alpha}{1-\epsilon\alpha}(2\lambda_1 + \lambda_0)$$

$$+ \frac{k_{tr}[M_0](1-\alpha)}{(1-\epsilon\alpha)}(\lambda_0 - \lambda_2) + \frac{\lambda_2\lambda_0\epsilon(1-\alpha)}{1-\epsilon\alpha}k_p$$

$$\frac{d\mu_0}{dt} = \frac{1}{2}k_t\lambda_0^2 + k_{tr}\frac{[M_0](1-\alpha)}{1-\epsilon\alpha}\lambda_0 + \frac{\mu_0\lambda_0\epsilon(1-\alpha)}{1-\epsilon\alpha}k_p$$

$$\frac{d\mu_1}{dt} = k_t\lambda_0\lambda_1 + k_{tr}\frac{[M_0](1-\alpha)}{1-\epsilon\alpha}\lambda_1 + \frac{\mu_1\lambda_0\epsilon(1-\alpha)}{1-\epsilon\alpha}k_p$$

$$\frac{d\mu_2}{dt} = k_t\left(\lambda_2\lambda_0 + \lambda_1^2\right) + k_{tr}\frac{[M_0](1-\alpha)}{1-\epsilon\alpha}\lambda_2 + \frac{\mu_2\lambda_0\epsilon(1-\alpha)}{1-\epsilon\alpha}k_p$$

where

$$\lambda_k = \sum_{n=1}^{\infty} n^k M_n \cdot$$

$$\mu_k = \sum_{n=1}^{\infty} n^k P_n$$

at $t = 0$, $\lambda_0 = \lambda_1 = \lambda_2 = \mu_0 = \mu_1 = \mu_2 = 0$

c. Simplified moment balance

$$\lambda_0 = \left(\frac{2fk_dI}{k_t}\right)^{1/2}$$

$$\lambda_1 = \frac{2fk_dI + k_p\lambda_0[M_0](1-\alpha)/(1-\epsilon\alpha) + \{k_{tr}[M_0](1-\alpha)/(1-\epsilon\alpha)\}\lambda_0}{k_t\lambda_0 + k_{tr}[M_0](1-\alpha)/(1-\epsilon\alpha)}$$

$$\lambda_2 = \frac{2fk_dI + \{k_p[M_0](1-\alpha)/(1-\epsilon\alpha)\}(2\lambda_1 + \lambda_0) + \{k_{tr}[M_0](1-\alpha)/(1-\epsilon\alpha)\}\lambda_0}{k_t\lambda_0 + k_{tr}[M_0](1-\alpha)/(1-\epsilon\alpha)}$$

$$\frac{d\mu_0}{dt} = \frac{1}{2}k_t\lambda_0^2 + k_{tr}\frac{[M_0](1-\alpha)}{1-\epsilon\alpha}\lambda_0$$

$$\frac{d\mu_1}{dt} = k_t\lambda_0\lambda_1 + k_{tr}\frac{[M_0](1-\alpha)}{1-\epsilon\alpha}\lambda_1$$

$$\frac{d\mu_2}{dt} = k_t\left(\lambda_2\lambda_0 + \lambda_1^2\right) + k_{tr}\frac{[M_0](1-\alpha)}{1-\epsilon\alpha}\lambda_2$$

at $t = 0$, $\mu_0 = \mu_1 = \mu_2 = 0$

d. Cumulative molecular weights

$$\langle\overline{M}_n\rangle = \left(\frac{\lambda_1 + \mu_1}{\lambda_0 + \mu_0}\right)M_0 \sim \left(\frac{\mu_1}{\mu_0}\right)M_0$$

$$\langle\overline{M}_w\rangle = \left(\frac{\lambda_2 + \mu_2}{\lambda_1 + \mu_1}\right)M_0 \sim \left(\frac{\mu_2}{\mu_1}\right)M_0$$

3. Constant density ρ, heat capacity C_p, heat conductivity k, and heat of reaction ΔH_R.

4. Mutual mass diffusion effects negligible.

With these assumptions, the basic equations of heat transfer can be written as:

Energy balance:

$$\rho C_p \frac{\partial T}{\partial t} = \underbrace{k\left[\frac{\partial^2 T}{\partial r^2} + \frac{1}{r}\frac{\partial T}{\partial r}\right]}_{\text{(conduction)}} + \underbrace{\rho \Delta H_R \frac{\partial \alpha}{\partial t}}_{\text{(generation)}} \tag{20}$$

Reaction:

$$\frac{\partial \alpha}{\partial t} = \frac{1-\alpha}{1\Big/\left\{\left[\pi_1 + (\pi_2\pi_3)^2\right]^{1/2} + \pi_2\pi_3\right\} + \pi_4} = R \tag{21}$$

with initial conditions

$$T = T_0 \qquad \text{at } t = 0 \qquad \text{for all } 0 \le r \le D/2 \tag{22}$$

$$\alpha = 0 \tag{23}$$

where D is the diameter of the reactor and T_0 is the initial material temperature.

The boundary conditions are

$$\frac{\partial T}{\partial r} = 0 \qquad \text{at } r = 0 \qquad \text{for } t > 0 \tag{24}$$

$$T = T_w \qquad \text{at } r = D/2 \qquad \text{for } t > 0 \tag{25}$$

where T_W is the wall temperature.

The reaction equation has the following constraints:

$$\frac{\partial \alpha}{\partial t} = 0 \qquad \text{for } t < t_z \tag{26}$$

$$\frac{\partial \alpha}{\partial t} = R \qquad \text{for } t \ge t_z \tag{27}$$

Equations (20)–(27) were solved by a numerical scheme which used the finite difference method for the space discretization and the first version of Gear's methods[47] for the time integration. Twenty equal increments were used in $0 \le r \le D/2$, and 41 ordinary differential equations were integrated using Gear's stiff ODE integrator to give local temperature, conversion, and reaction rate profiles. For the styrene reactions, molecular weights were calculated

using either eqs. (16)–(19) or equations listed in Tables IV(c) and IV(d). Further details of the numerical techniques are available from the authors.

Model Prediction

DSC

The lumped sum parameters π_1, π_2, π_3, and π_4 were determined step by step from isothermal DSC experiments by either graphical or analytical procedures.[35] A list of numerical values used in the model prediction is given in Tables V (styrene) and VI (polyester). The predicted rate of reaction vs. time curves and conversion profiles of isothermal DSC experiments are shown in Figure 2 for the styrene reaction and Figures 3 and 4 for the polyester reaction. The model predicts the profiles very well. For styrene reactions, the predicted curves rose sharply at the beginning of the reaction primarily as a consequence of the model assumption that polymerization started instantaneously when the inhibitor was completely consumed. Following this were conventional kinetics, gel effect, and limiting conversion regions. On the other hand, due to the lack of kinetic controlled region for polyester reaction as mentioned earlier, the reaction commenced under the diffusion effect, which caused the rate increase at the initial stage. Kinetic information can be further explained by plotting modified reaction rate, apparent propagation rate constant k_p, and free radical concentration $M \cdot$ vs. conversion. The modified reaction rate is essentially the reaction rate corrected for the consumption of monomer and henceforth is equivalent to a product of apparent propagation rate constant and free radical concentration. Figure 10 shows that for styrene reaction at low temperatures (i.e., 60–100°C), the free radical concentration was an increasing function of conversion. At low conversions, the free radical concentration was higher at higher temperature due to the temperature effect, while, at high conversions, it was higher at lower temperature due to the gel effect. On the other hand, the apparent propagation rate constant remained unaltered except for exhibiting a drastic decline due to the glass transition at the final stage. The combined effect shows that the modified rate profile started with a flat region, followed by an increase, and ended with an abrupt drop. Figure 11 shows the simulation results for the same reaction over high temperature ranges (i.e., 110–150°C), assuming that thermal initiation is negligible. At 110°C the gel effect and glass transition phenomenon were still observed as evidenced by a sharp increase in free radical concentration and a drastic drop in apparent propagation rate constant at the later stage of reaction, while at higher temperatures both phenomena disappeared. Instead, the result reveals that despite the fact that the calculated propagation rate constant was maintained constant and was higher at higher temperatures throughout the reaction, the calculated free radical concentration was severely curtailed at higher temperatures, thereby an incomplete reaction resulted as a consequence of the fast depletion of initiator known as dead-ending phenomenon. Model prediction shows that polyester reactions are incomplete (see Figs. 4 and 6) due to the glass transition effect[50,51] at 60–100°C and to the dead-ending phenomenon at 100–120°C.

TABLE V
Numerical Values of Parameters Used in Model Prediction (Styrene)

a. Kinetics[35]

$$k_d\ (\text{min}^{-1}) = 5.9 \times 10^{14} \exp(-28400/RT)$$

$$T_{gP} = 366.7\ \text{K}$$

$$T_{gM} = 185.0\ \text{K}$$

$$\beta_P = 0.00048$$

$$\beta_M = 0.001$$

$$\lambda = 1 \qquad \text{for } T \geq 85°\text{C}$$

$$\lambda = 0.3 \qquad \text{for } T < 85°\text{C}$$

$$d_p\ (\text{g/cm}^3) = 1.084 - 0.000605(T - 273.2)$$

$$d_M\ (\text{g/cm}^3) = 0.924 - 0.000918(T - 273.2)$$

$$2f\bar{I}_0 k_{p0} F\ (\text{min}^{-1}) = 0.01 \exp(2681/RT)$$

$$2f\bar{I}_0 k_d k_{p0}^2/k_{t0}\ (\text{min}^{-2}) = 1.8 \times 10^{23} \exp(-45214/RT)$$

$$A_M\ (\text{min}) = 2.73 \times 10^{11} \exp(-27454/RT)$$

$$B_M = 0.42$$

$$B_p = 0.01837$$

$$A_p/F\ (\text{min}) = \exp\left[a' + b'\left(\ln 1/V_f - \ln 1/\bar{V}_{f0}\right) + c'\left(\ln 1/V_f - \ln 1/\bar{V}_{f0}\right)^2\right]$$

where

$$a' = -14.83 + 6845/T$$

$$b' = -14.17 + 5213/T$$

$$c' = -8.56 + 2473/T$$

$$\ln 1/\bar{V}_{f0} = 3.2824$$

b. Molecular weights

	Reference
$C_M = 1.00 \exp(-3212/T)$	45
$f = 1.0$	
$[\text{I}_0] = 0.1082$ mol/L	
$[\text{M}_0] = 8.6635$ mol/L	
$k_{p0} = 7.138 \times 10^9 \exp(-5616/T)$ $(\text{s}^{-1}\ M^{-1})$	48
c. Heat transfer	
$\rho = 0.9$ g/cm^3	49
$c_p = 0.405$ cal/g °C	49
$k = 2.07 \times 10^{-2}$ cal/cm °C min	49
$\Delta H_R = 158$ cal/g	15

TABLE VI
Numerical Values of Parameters Used in Model Prediction (Polyester)

a. Kinetics

$$k_d\ (\mathrm{s}^{-1}) = 1.0102 \times 10^{14}\exp(-29344/RT)$$

$$T_{gP} = 369.96\ \mathrm{K}$$

$$T_{gM} = 258.04\ \mathrm{K}$$

$$\beta_p = 0.00048$$

$$\beta_M = 0.001$$

$$\lambda = 1$$

$$\epsilon = 0$$

$$2f\bar{I}_0 k_{p0} F\ (\mathrm{s}^{-1}) = 1.01 \times 10^5\exp(-4549.71/T)$$

$$2f\bar{I}_0 k_d k_{p0}^2/k_{t0}\ (\mathrm{s}^{-2}) = 0$$

$$A_M\ (\mathrm{s}) = 7.02 \times 10^{-14}\exp(12764.61/T)$$

$$B_M = 0.03$$

$$B_p = 1.0$$

$$A_p/F\ (\mathrm{s}) = \exp\left[a' + b'\ln 1/V_f + c'(\ln 1/V_f)^2\right]$$

where

$$a' = 916.91 - 356141/T$$

$$b' = -614.33 + 243573/T$$

$$c' = 95.45 - 39511.2/T$$

b. Heat transfer[4]

$$\rho = 1.1\ \mathrm{g/cm^3}$$

$$c_p = 0.4\ \mathrm{cal/g\ °C}$$

$$k = 0.024\ \mathrm{cal/cm\ °C\ min}$$

$$\Delta H_R = 50.0\ \mathrm{cal/g}$$

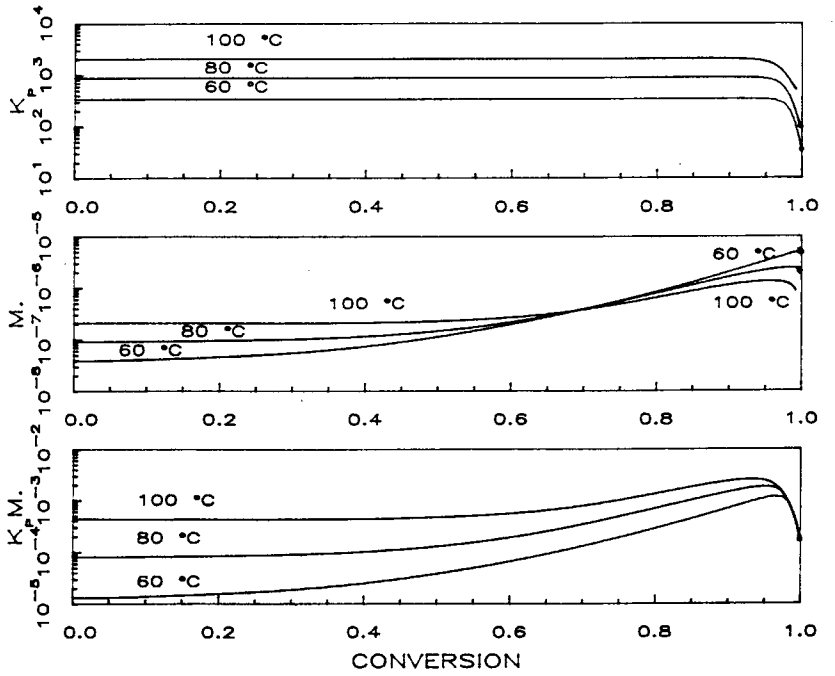

Fig. 10. Calculated apparent propagation rate constant, free radical concentration, and modified reaction rate vs. conversion for isothermal styrene reaction initiated by BPO at 60–100°C.

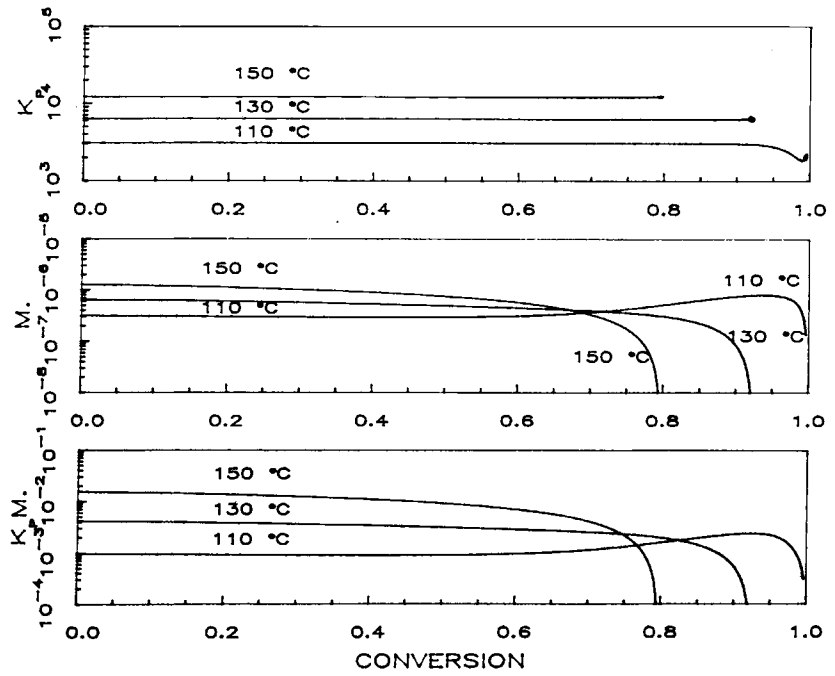

Fig. 11. Calculated apparent propagation rate constant, free radical concentration, and modified reaction rate vs. conversion for isothermal styrene reaction initiated by BPO at 110–150°C.

Batch Casting

Thermal properties used to calculate the temperature profile during the casting process are listed in Tables V (styrene) and VI (polyester), where the heat reaction ΔH_R was determined from the DSC experiments. The predicted temperature curves compare reasonably well with the experimental data in Figure 7 (polyester) and in Figures 8 and 9 (styrene). Since the thermocouple beads have a substantial size (~ 1 mm in diameter), the measured temperature profiles reflect an average temperature for a volume rather than a point value. Therefore, near the wall where the temperature gradient was sharp, calculated temperatures were apt to deviation from experimental data.

Figure 7 shows that the predicted conversion is incomplete for the casting of polyester both at the center (94%) and near the wall (89%). The former is due to the dead-ending phenomenon while the latter is due to the glass transition effect. DSC measurements, however, revealed only less than 3% residual reactivity near the wall and no residual reactivity at the center. This discrepancy may partially result from the insensitivity of DSC measurements at high conversions and the inaccuracy of the kinetic model when the kinetic parameters were extrapolated to higher temperatures.

Figure 12 shows the simulation curves of cumulative molecular weights vs. conversion for the casting of styrene at 75°C. The molecular weights increase appreciably at the late stage of reaction due to the gel effect. As expected, the molecular weights of the material near the wall, which is in the low temperature region, are higher than those at the center. Figure 13 shows the comparison of cumulative weight average molecular weights between two different wall temperature programs. When the wall temperature is raised from 75 to

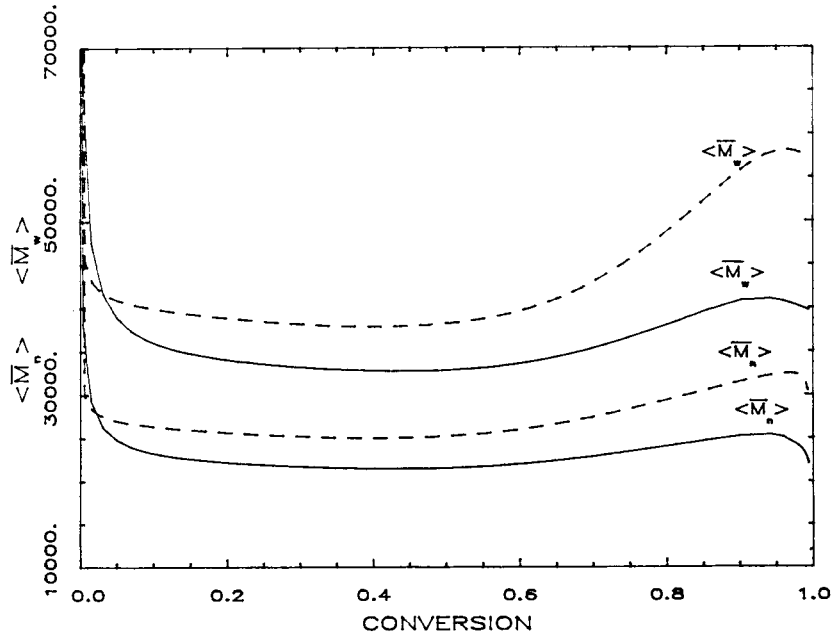

Fig. 12. Calculated local cumulative molecular weights vs. conversion for the casting of styrene, T_w = 75°C, diameter = 3/4 in.: (---) near wall; (—) at center.

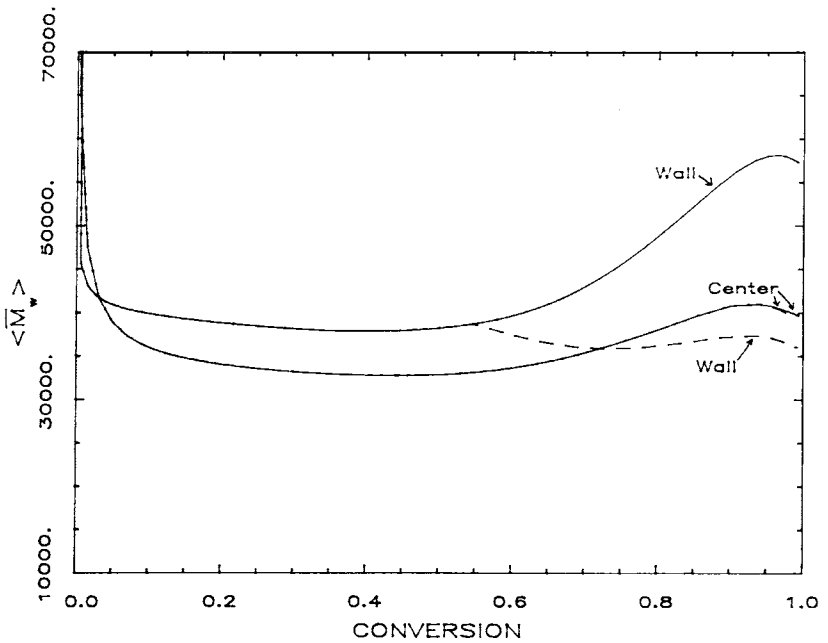

Fig. 13. Comparison of calculated local cumulative weight average molecular weights vs. conversion for different wall temperature programs, diameter = 3/4 in.: (—) T_w = 75°C; (---) T_w = 75–90°C.

90°C, the molecular weight near the wall decreases, while the molecular weight at the center is almost unchanged. This can be explained by the fact that at the time of temperature switchover, the conversions have already reached 95% at the center but only 55% near the wall [see Fig. 9(a)]. Furthermore, the reacting material near the wall may response to the wall temperature change much faster than that at the center. As a result, the molecular weight experiences a substantial drop near the wall but only a slight decrease at the center. It is of interest to notice that the variation of molecular weights in the radical direction is thereby reversed, with a higher molecular weight at the center than near the wall. This is demonstrated by the experimental data listed in Table III.

Table III shows the comparison between the experimental and calculated molecular weights for the casting of styrene under different wall temperature programs. Using the literature data[45,48] for molecular parameters, the experimental and calculated values reveal some deviation, but are in the same order of magnitude. The general trend of the molecular weight changes is correctly predicted by the model. Discrepancies between the experimental and calculated results may result from the experimental error since the sample collected for the GPC analysis represents an area instead of a single point. Therefore, the measured molecular weights reflect only average values near the location of interest.

In our kinetic-diffusion model, the pseudo-steady state assumption (QSSA) for radicals[37] was made. It has been shown that[14] for PMMA bulk polymerizations, which are characterized by a very strong gel effect, the QSSA for

radicals may lead to an appreciable deviation in predicting the free radical concentration and molecular weights. This is, however, not the case in styrene polymerizations, which exhibit only a moderate gel effect. The kinetic parameters calculated by assuming no QSSA have been employed to predict reaction rate, free radical concentration, and molecular weights in a broad temperature range from 75 to 150°C for styrene reaction. The comparison between the two cases, i.e., with and without QSSA for radicals, showed an excellent agreement. The molecular weight calculations based on either instantaneous kinetic chain length concept or the method of moments also showed little distinction.

CONCLUSIONS

A kinetic-diffusion model has been proposed for free radical bulk polymerizations. This model can simulate not only reaction rate and conversion, but also gel effect, glass effect, and dead-ending phenomenon. It can be employed under nonisothermal conditions as well. Model predictions of temperature profiles, limiting conversion and molecular weights have shown reasonable agreement with experimental results for the batch casting of styrene and an unsaturated polyester resin. Both experimental results and model prediction showed that the temperature gradient might lead to a molecular weight variation in the radical direction which could be enhanced or reduced by means of manipulating the wall temperature during the polymerization.

The authors would like to thank General Motors and Amoco Foundation for financial support. Material donation from Owens Corning Fiberglas Co. is greatly appreciated.

APPENDIX: NOMENCLATURE

A_M	A'/A'_M
A_p	A''/A'_p
A', A'_M, B_M	parameters for monomer diffusion
A'', A'_p, B_p	parameters for polymer diffusion
a'	parameter for polymer diffusion
b'	parameter for polymer diffusion
C_M	chain transfer constant to monomer
C_p	heat capacity
c'	parameter for polymer diffusion
D	diameter
D_M	self-diffusivity of monomer
D_p	self-diffusivity of polymer
d_m	density of monomer
d_p	density of polymer
f	initiator efficiency
F	lumped kinetic parameter for diffusion-affected propagation
ΔH_R	heat of reaction
I	initiator (concentration)
I_0	initial initiator concentration
$[I_0]$	initial initiator concentration
$\bar{I}_0$	initiator concentration after all inhibitors have been consumed
k	thermal conductivity
k_d	initiator decomposition rate constant
k_i	initiation rate constant
k_p	propagation rate constant
k_{p0}	true propagation rate constant

k_t	termination rate constant
k_{tr}	rate constant for chain transfer to monomer
k_{t0}	true termination rate constant
k_z	inhibition rate constant
M	monomer (concentration)
M_j	growing polymer radical with degree of polymerization j (concentration)
M	$\sum_{j=1}^{\infty} M_j \cdot$, total radical concentration
M_0	molecular weight of monomer (= 104 for styrene)
$[M_0]$	initial concentration of monomer
$\overline{M}_n$	instantaneous number average molecular weight
$\overline{M}_w$	instantaneous weight average molecular weight
$\langle \overline{M}_n \rangle$	cumulative number average molecular weight
$\langle \overline{M}_w \rangle$	cumulative weight average molecular weight
P_j	dead polymer with degree of polymerization, j
q	inhibitor efficiency
R	primary initiator radical or reaction rate
r	radius
T	temperature
T_c	center temperature
T_{gM}	glass transition temperature for monomer
T_{gP}	glass transition temperature for polymer
T_w	wall temperature
t	time
t_z	induction time
V_f	free volume fraction
V_{f0}	parameter for polymer diffusion
$\overline{X}_n$	instantaneous number average degree of polymerization
$\overline{X}_w$	instantaneous weight average degree of polymerization
x_c	conversion at the center
x_w	conversion near the wall
Z	inhibitor
z_0	initial inhibitor concentration

Greek Letters

α	fractional conversion
β	reciprocal of kinetic chain length
β_M	difference of thermal expansion coefficients above and below T_g for monomer
β_p	difference of thermal expansion coefficients above and below T_g for polymer
ϵ	$(d_p - d_m)/d_p$ volume contraction coefficient
λ	numerical factor of ϵ due to glass transition
λ_i	ith moment of living polymer concentration
μ_i	ith moment of dead polymer concentration
ρ	density of reacting system
τ	chain transfer constant to monomer
$\pi_1, \pi_2, \pi_3, \pi_4$	lumped-sum parameters defined in eq. (10)

References

1. E. Broyer and C. W. Macosko, *AIChE J.*, **22**, 268 (1976).
2. R. T. Ross and R. L. Laurence, *AIChE Symp. Ser.*, **72**, 80 (1976).
3. S. Kovenklioglu, *Polym. Eng. Sci.*, **20**, 816 (1980).
4. L. J. Lee, *Polym. Eng. Sci.*, **21**, 483 (1981).
5. S. R. Estevez and J. M. Castro, *Polym. Eng. Sci.*, **24**, 428 (1984).
6. J. A. Biesenberger and R. Capinpin, *Polym. Eng. Sci.*, **14**, 737 (1974).
7. J. A. Biesenberger and R. Capinpin, and D. Sebastian, *Appl. Polym. Symp.*, **26**, 211 (1975).
8. J. A. Biesenberger, R. Capinpin, and J. C. Yang, *Polym. Eng. Sci.*, **16**, 101 (1976).
9. D. H. Sebastian and J. A. Biesenberger, *Polym. Eng. Sci.*, **16**, 117 (1976).

10. J. A. Biesenberger and D. H. Sebastian, *Principles of Polymerization Engineering*, Wiley, New York, 1983, Chap. 4.
11. A. V. Tobolsky, *J. Am. Chem. Soc.*, **80**, 5927 (1958).
12. V. E. Trommsdorff, H. Kohle, and P. Lagally, *Makromol. Chem.*, **1**, 169 (1947).
13. P. E. Baillagou and D. S. Soong, *Chem. Eng. Sci.*, **40**, 75 (1985).
14. W. Y. Chiu, G. M. Carratt, and D. S. Soong, *Macromolecules*, **16**, 348 (1983).
15. Y. J. Huang and L. J. Lee, *AIChE J.*, **31**, 1585 (1985).
16. M. E. Sacks, S. Lee, and J. A. Biesenberger, *Chem. Eng. Sci.*, **27**, 2281 (1972).
17. M. E. Sacks, S. Lee, and J. A. Biesenberger, *Chem. Eng. Sci.*, **28**, 241 (1973).
18. S. Chen and W. Jeng, *Chem. Eng. Sci.*, **33**, 735 (1978).
19. S. Chen and K. Lin, *Chem. Eng. Sci.*, **35**, 2325 (1980).
20. S. Chen and K. Hsu, *Chem. Eng. Sci.*, **39**, 177 (1984).
21. G. Z. A. Wu, L. A. Denton, and R. L. Laurence, *Polym. Eng. Sci.*, **22**, 1 (1982).
22. B. M. Louie, and D. S. Soong, *J. Appl. Polym. Sci.*, **30**, 3707 (1985).
23. S. Lynn and J. E. Huff, *AIChE J.*, **17**, 475 (1971).
24. J. P. A. Wallis, R. A. Ritter, and H. Andre, *AIChE J.*, **21**, 686 (1975).
25. J. P. A. Wallis, R. A. Ritter, and H. Andre, *AIChE J.*, **21**, 691 (1975).
26. S. Lynn, *AIChE J.*, **23**, 387 (1977).
27. R. Cintron-Cordero, R. A. Mostello, and J. A. Biesenberger, *Can. J. Chem. Eng.*, **46**, 434 (1968).
28. C. E. Wyman and L. F. Carter, *AIChE Symp. Ser.*, **72**, 1 (1976).
29. L. Valsamis and J. A. Biesenberger, *AIChE Symp. Ser.*, **72**, 18 (1976).
30. M. Ghosh, D. W. Foster, J. P. Lenczyk, and T. H. Forsyth, *AIChE Symp. Ser.*, **72**, 102 (1976).
31. A. Husain and A. E. Hamielec, *AIChE Symp. Ser.*, **72**, 112 (1976).
32. P. E. Baillagou and D. S. Soong, *Polym. Eng. Sci.*, **25**, 212 (1985).
33. P. E. Baillagou and D. S. Soong, *Polym. Eng. Sci.*, **25**, 232 (1985).
34. E. A. Collins, J. Bares, and F. W. Billmeyer, *Experiment in Polymer Science*, Wiley, New York, 1973, p. 339.
35. Y. J. Huang, M.S. thesis, Ohio State University, 1983.
36. J. F. Stevenson, *SPE ANTEC Papers*, **26**, 452 (1980).
37. J. A. Biesenberger and R. Capinpin, *J. Appl. Polym. Sci.*, **16**, 695 (1972).
38. W. H. Ray, *J. Macromol. Sci., Rev. Macromol. Chem.*, **C8**, 1 (1972).
39. J. N. Cardenas and K. F. O'Driscoll, *J. Polym. Sci., Polym. Chem. Ed.*, **14**, 883 (1976).
40. R. T. Ross and R. L. Laurence, *AIChE Symp. Ser.*, **72**, 74 (1976).
41. K. Arai and S. Saito, *J. Chem. Eng., Jpn.*, **9**, 302 (1976).
42. A. D. Schmidt and W. H. Ray, *Chem. Eng. Sci.*, **36**, 1401 (1981).
43. T. J. Tulig and M. Tirrell, *Macromolecules*, **14**, 1501 (1981).
44. S. T. Balke and A. E. Hamielec, *J. Appl. Polym. Sci.*, **17**, 905 (1973).
45. F. L. Marten and A. E. Hamielec, *J. Appl. Polym. Sci.*, **27**, 489 (1982).
46. S. K. Soh and D. C. Sundberg, *J. Polym. Sci., Polym. Chem. Ed.*, **20**, 1299 (1982).
47. C. W. Gear, *Communications of the Association for Computing Machinery (ACM)*, **14**, 185 (1971).
48. J. Brandrup and E. H. Immergut, *Polymer Handbook*, 2nd ed., Wiley, New York, 1975.
49. R. W. Gallant, *Hydrocarbon Process.*, **49**, 112 (1970).
50. K. Horie, I. Mita, and H. Kambe, *J. Polym. Sci., Part A-1*, **6**, 2663 (1968).
51. K. Horie, I. Mita, and H. Kambe, *J. Polym. Sci., Part A-1*, **8**, 2839 (1970).

Received July 16, 1986
Accepted July 21, 1986